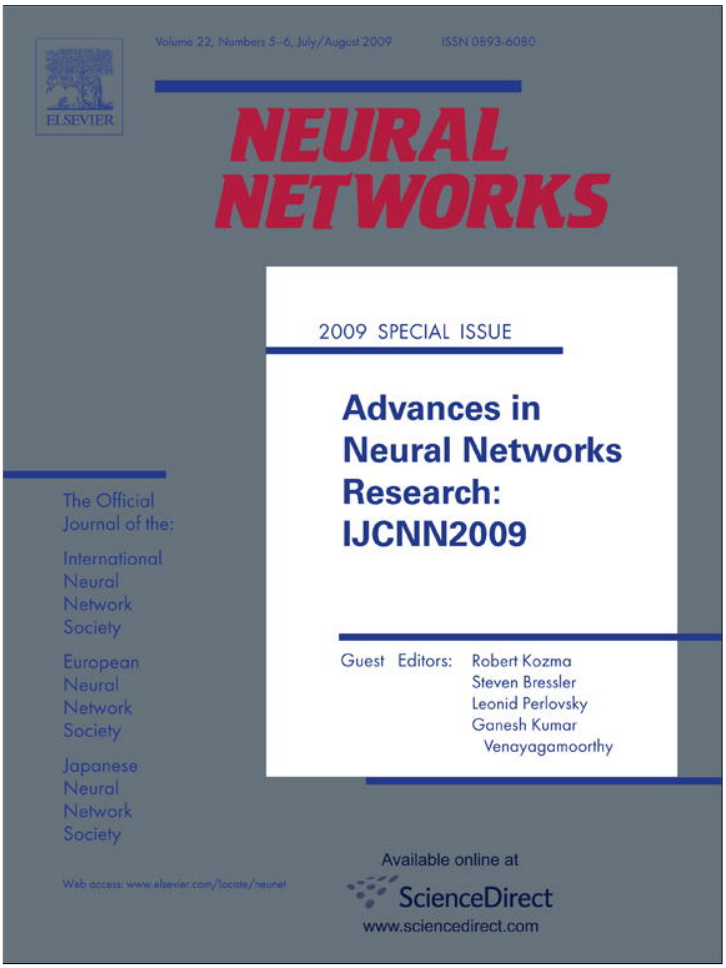

Neural Networks 22 (2009) 491–501

Contents lists available at ScienceDirect

Neural Networks

journal homepage: www.elsevier.com/locate/neunet

2009 Special Issue

Vortices in brain activity: Their mechanism and significance for perception

Walter J. Freeman *

Department of Molecular & Cell Biology, Donner 101, University of California, Berkeley CA 94720-3206, United States

ARTICLE INFO

Article history:
Received 2 May 2009
Received in revised form 19 May 2009
Accepted 25 June 2009

Keywords:
AM pattern
Background spontaneous activity
ECoG
Gamma oscillations
Null spike
Perception
Phase cone
Phase transition
Rayleigh and Rice distributions
Symmetry breaking
Theta–gamma linkage
Vortex

ABSTRACT

Brains interface with the world through perception. The process extracts information from microscopic sensory inputs and incorporates it into the mesoscopic memory store for retrieval in recognition. The process requires creation of spatiotemporal patterns of neural activity. The construction is done through phase transitions in cortical populations that condense the background activity through spontaneous symmetry breaking. Large-scale interactions create fields of synaptically driven activity that is observed by measuring brain waves (electrocorticogram, ECoG) and evaluated by constructing a mesoscopic vectorial order parameter as follows. The negative feedback among excitatory and inhibitory neurons creates spatially and spectrally distributed gamma oscillations (20–80 Hz) in the background activity. Band pass filtering reveals beats in ECoG log analytic power. In some beats that recur at theta rates (3–7 Hz), the order parameter transiently approaches zero, giving a null spike in which the microscopic activity is uniformly disordered (symmetric). A phase transition that is manifested in an analytic phase discontinuity breaks the symmetry. As the null spike terminates, the resurgent order parameter imposes mesoscopic order seen in spatial patterns of ECoG amplitude modulation (AM) that actualize and update the memory of a stimulus. Read-out is through a divergent/convergent projection that performs on cortical output an irreversible spatiotemporal integral transformation. The ECoG reveals a conic phase gradient that accompanies an AM pattern. The phase cone manifests a vortex, which is initiated by the null spike, and which is inferred to help stabilize and prolong its accompanying AM pattern that might otherwise be rapidly degraded by the turbulent neural noise from which it emerges.

1. Introduction

Brains constantly generate background activity whether they are at work, rest or in sleep (Freeman, 2009a). The activity is seen in the continuous irregular firing of action potentials at the microscopic level, in fluctuating dendritic potentials at the mesoscopic level, and in spatiotemporal fluctuations in blood flow at the macroscopic level, which indirectly reflect the insatiable demands of brains for energy. It is commonly regarded as chaos, but it is not deterministic chaos (Rapp, 1993), because those systems are stationary, autonomous and noise-free, whereas brains are noisy, time-varying, open systems generating *stochastic chaos* (Freeman, 2000; Freeman, Kozma, & Werbos, 2001; Kozma, Puljic, Balister, Bollabás, & Freeman, 2005). It is also regarded as noise and removed by time-locked averaging to extract event-related potentials, on the assumption that the stimulus- or response-related activity is superimposed on the background activity. However, the background activity is neither random nor chaotic but is self-organized in dynamic structures that reflect the properties of neural mechanisms by which brains regulate themselves close to criticality, and by which they reorganize in transitions from rest to work (Freeman, 2004a, 2004b, 2005, 2006; Makeig et al., 2002).

This review is focused on four spatiotemporal structures in the background activity, which have been observed in the band pass filtered electrocorticogram (ECoG) of cortices at rest and at work. One appears as a power-law spectrum. Another is a temporal downward spike in the analytic power of electric potential, decreasing often by a factor of 10^{-4} to 10^{-6}. The third is a stable spatial pattern of the analytic phase with respect to the mean phase at the center frequency of the pass band, which has the form of a cone. The fourth is pulsing or rotating patterns of ECoG amplitude, which are displayed in successive movie frames of digitized, band pass filtered data from 8 × 8 electrode arrays (6 × 6 mm in rabbit; 10 × 10 mm in human) on the cortical surface. These patterns resemble satellite video images of the vortex of a hurricane.

Reasons are given in this essay for proposing that these several structures are different manifestations of the process in the cortex by which perception reads out memories. The memories are stored by learning in cortical synaptic webs, and the read-out is triggered by conditioned stimuli through a process that is characterized as a phase transition (Freeman, 1990; Kozma & Freeman, 2001; Kozma et al., 2005) in cortical dynamics. The read-out results in a spatial pattern of amplitude modulation (AM) of the carrier frequency in

* Tel.: +1 510 642 4220; fax: +1 510 643 9290.
E-mail address: dfreeman@berkeley.edu.
URL: http://www.sulcus.berkeley.edu.

0893-6080/$ – see front matter © 2009 Elsevier Ltd. All rights reserved.
doi:10.1016/j.neunet.2009.06.050

the beta or gamma ECoG frequency range. It is classifiable with respect to triggering stimuli (Freeman, 2005). An accompanying spatial pattern of phase modulation (PM) of the carrier wave has no classificatory value, though it serves to define and widen the temporal boundaries of the AM pattern (Freeman, 2006).

Section 2 summarizes experimental observations. Section 3 introduces the Rice distribution. Section 4 proposes that background activity is sustained by mutual excitation. Section 5 proposes that inhibitory feedback operates as a band pass filter. Section 6 postulates governance of cortex by an occult limit cycle attractor. Section 7 concludes with remarks on the neural mechanisms of perception.

2. Power-law PSD, null spikes, phase cones, vortices

Microscopic background activity that is observed in the extracellular recording of axonal action potentials with audio and visual monitors resembles *white noise* with equal power density across the spectrum. The power spectral density (PSD) in log–log coordinates is a power-law distribution with slope = 0, $1/f^0$ (flat spectrum = white noise) but only up to one or more kHz. Above that *break frequency* is pink noise, $1/f$ of slope −1. Mesoscopic ECoG is from synaptic currents of dendrites that cumulatively sum the synaptic potentials evoked by the action potentials. The cumulative sum of white noise with zero mean is *brown* noise with a slope of −2, $1/f^2$. The PSD of summed extracellular dendritic potentials that provide the main constituents of the ECoG in awake rest approaches brown noise with an average slope near −2, but owing to refractory periods the slope is steeper; in deep slow wave sleep the slope averages near −3 (Fig. 1) (Freeman, 2009b; Freeman, Holmes, West, & Vanhatalo, 2006).

The important generalization is that the spectra of the mesoscopic rest ECoG are continuous and power-law for all slopes between −2 and −4 (Freeman & Zhai, 2009). The implied self-similarity has been confirmed over the spectral ranges of clinical interest: theta, alpha, beta, and gamma (Freeman, 2007a; Freeman, O'Nuillain, & Rodriguez, 2008). The obvious inference is that a band pass filter of any center frequency and bandwidth applied to ECoG will give Rayleigh noise (Fig. 2A, B), as already found in olfactory cortical ECoG (Fig. 3.13c, p. 148 in Freeman (1975)).

The statistical properties of the beats are best revealed by the logarithm of the analytic power (the square of the analytic amplitude following the Hilbert transform (Freeman, 2007b)) (Fig. 2C) and the analytic frequency (D), which is approximated by calculating the differences between successive digitizing steps in radians, dividing them by the duration of the digitizing step in s, and dividing by 2π to get the instantaneous analytic frequency in Hz.

The similarity held for differing pass bandwidths and center frequencies and equally for brown and black noises with various slopes (Freeman & Zhai, 2009) for human, cat and rabbit ECoG.

Histograms were calculated of the intervals between events where successive power differences changed from negative to positive, indicating a down spike. Ripples imposed by digital filtering gave a bimodal histogram owing to the very short intervals. Demeaning and setting a threshold at the minimum of the histogram between the two maxima minimized distortion. The modes of the valid intervals were found to depend only on the width of the pass band irrespective of the center frequency, again underscoring the self-similarity of the resting ECoG. Rice (1945), Breiman (1968) and Papoulis and Pillai (2002) predicted this result for white noise. Simulations confirmed his result before extension of his procedure to brown and black noises and to ECoG. Comparison among the four data sets proved their similarity for resting ECoG (see Fig. 7A below). Rice proved that the modal values from white noise expressed as the beat frequency in Hz were

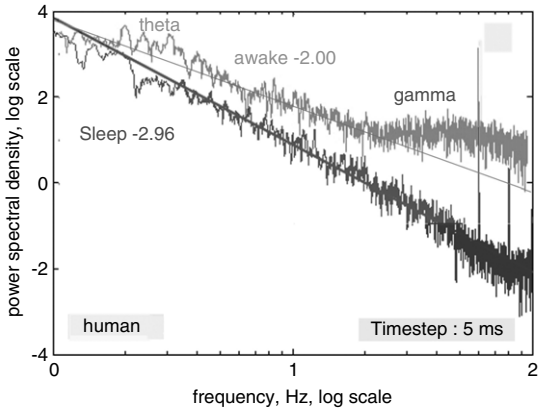

Fig. 1. The power spectral density (PSD) is illustrated for the transition from slow wave sleep to active arousal. The power-law distribution of spectral energy reflects both the randomness of the background activity at rest and the self-similarity across a broad range of oscillations. The steep slope of black noise (log–log PSD slope a in $1/f^a = -4 < a < -2$) is explained by the refractory periods of the neurons generating the background activity. In waking rest the slope shifts toward −2. Upon active engagement with the environment, peaks emerge above the power-law level (Freeman, 2006, 2007a; Freeman & Zhai, 2009), curve fitting by linear regression with the criterion of least squares residuals indicates a slope shallower than −2, but with excessive residuals (Freeman, 2009b).

proportional to the bandwidth in Hz by a factor of 0.641 (Sect. 3.8., page 90, equation 3.8–3.15 in Rice (1945)). This value was confirmed for human ECoG, rabbit ECoG, and simulated brown and black noises (see Fig. 5 in Freeman (2009b)).

The histograms giving the distributions of values of the logarithm of analytic power revealed the similarity of the derivations from brown noise (Fig. 3A) and ECoG (B).

The spatial pattern of phase modulation (PM) from the 8 × 8 phase values that accompanied the AM pattern of the carrier wave at its relatively fixed frequency had the shape of a cone in the cortical surface coordinates. In a view onto the surface (Fig. 4) the isophase contours of an example appear as arcs (steps of 0.1 rad). The location and sign (lag 'o' or lead '•') of the cone varied randomly from each AM pattern to the next but were fixed within AM patterns. The phase gradient in rad/mm of the cone varied randomly inversely with the carrier frequency in rad/s; the mean phase velocity from the ratio in m/s equaled mean conduction velocity of cortical axons running parallel to the surface (Freeman & Baird, 1987). Maps of the phase cones on the cortical surface showed that the frames lasted 3 to 5 cycles of the carrier oscillation. The phase cone helped to determine the location, diameter, starting time and duration of each frame containing an AM pattern, but it has no classificatory value with respect to stimuli (Freeman, 2005, 2006).

Display of the filtered ECoG amplitude by frames at twice the digitizing interval in movies showed overlapping AM patterns with different locations, carrier frequencies, and PM patterns. An example (Fig. 5) looking through the 6 × 6 mm array window onto the cortical surface shows one focus that oscillates with repeated expansion of alternating positive and negative peaks (+o − o+). The other focus oscillates with alternating positive and negative peaks (PNPN) rotating counterclockwise about a fixed point corresponding to the downward apex of a phase cone with maximal lag (implosion). This technique showed that the conic phase gradients were time-dependent (Kozma & Freeman, 2008) as schematized in Fig. 6; six types of spatial PM patterns were observed: repetitive expansion (explosion), contraction (implosion), clockwise rotation, or counterclockwise rotation (Freeman & Vitiello, 2009).

3. The appearance of Rice noise

The down spike interval histograms from both rabbit and human at rest conformed to the Rayleigh distribution (Fig. 7A) for

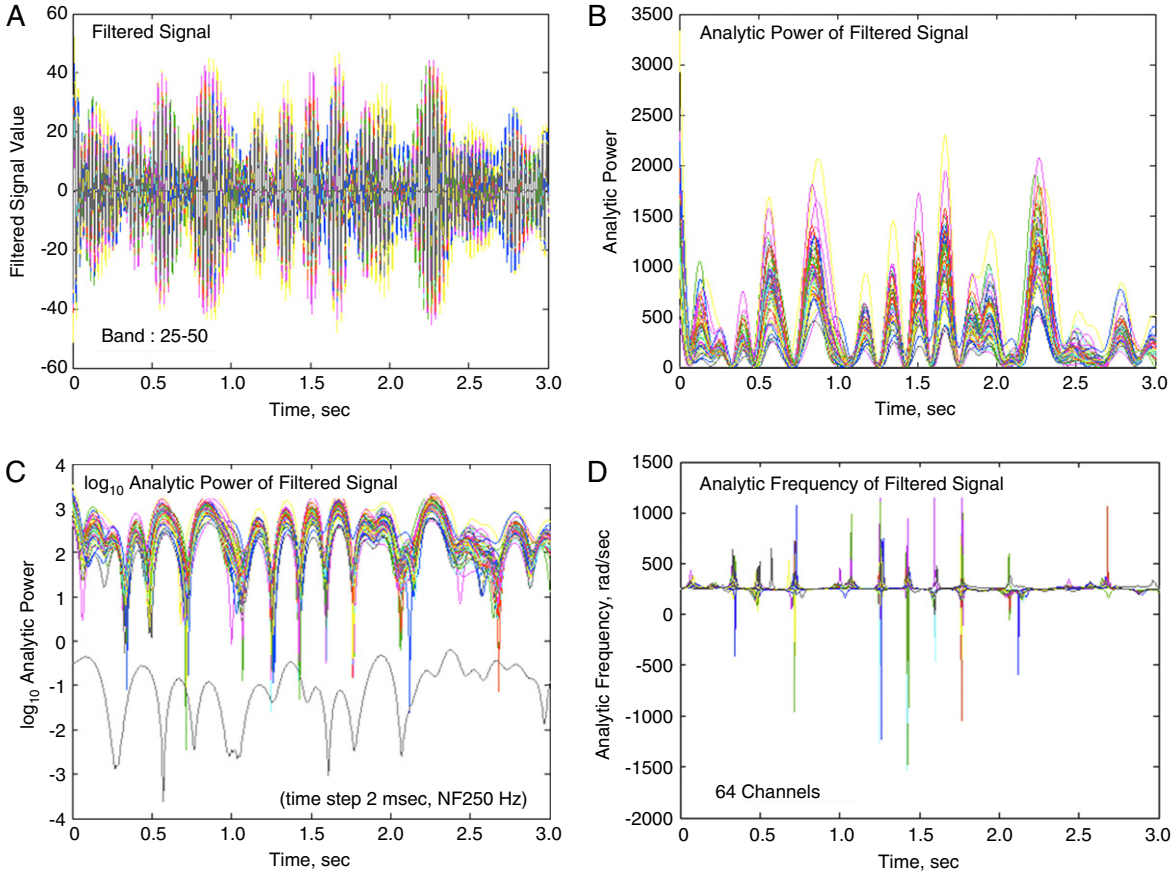

Fig. 2. A. Application of a band pass filter, here in the low gamma range 25–50 Hz, to resting ECoG produces beats in Rayleigh noise. This recording from an 8×8 electrode array (5.6×5.6 mm) on rabbit visual cortex shows 64 superimposed ECoG signals. B. Application of the Hilbert transform gives the analytic power of the 64 signals, showing the repeated approach to zero power (Freeman, 2009b; Freeman et al., 2008). C. The logarithm of the analytic power shows sharp down spikes in clusters among the 64 signals. The lower line shows a defective channel D. The analytic frequency shows positive and negative spikes during the down spikes where the analytic phase is indeterminate. Null spikes were down $< 10^{-4}$. At these times the spatial standard deviation, $SD_X(t)$, has high values. Each epoch between spikes has a minimum in $SD_X(t)$ that serves to evaluate the analytic frequency distribution in the epoch. The mean analytic frequency is nearly constant in each epoch and on average shifts by ± 10 Hz between epochs. The lower signal in C is from a blocked electrode (Freeman, 2009b).

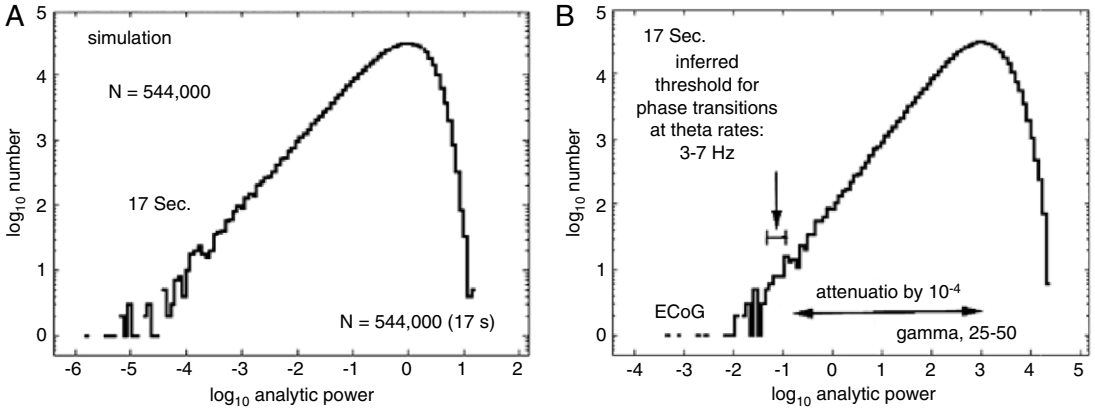

Fig. 3. The distributions of the logarithm of analytic power were calculated from a 17 s continuous record from 64 electrodes at 2 ms intervals (B) for comparison with 64 simulated independent time series. The pass band was in the low gamma range (Freeman & Zhai, 2009). Spikes less than the inferred threshold are referred to as null spikes.

all center frequencies tested, as Rice (1945) predicted for white noise, provided that the bandwidth exceeded 8 Hz. For bandwidths of 3 to 6 Hz and sometimes up to 8 Hz a different distribution was observed, which it turned out Rice (1945) had also predicted. When he added a sine wave to white noise, the modal value of interval distributions from the 4 Hz band pass filtered ECoG increased toward almost twice the Rayleigh mode (Fig. 7B), depending on the amplitude of the added sine wave, at the sine wave frequency. In 4 Hz pass bands on the shoulders, the modal interval was shorter (Fig. 8A). The modified distributions can be called examples of the Rice distribution. Rice proposed using this effect to locate signals embedded in random noise. Here it was considered possible to serve that purpose in the search for signals in ECoG and possibly EEG.

The search for a comparable shift in distribution in rabbits engaged in responding to conditioned stimuli yielded similar shifts in 4 Hz bands with center frequencies ranging from 16 to 88 Hz, although the deviations from the Rayleigh distribution

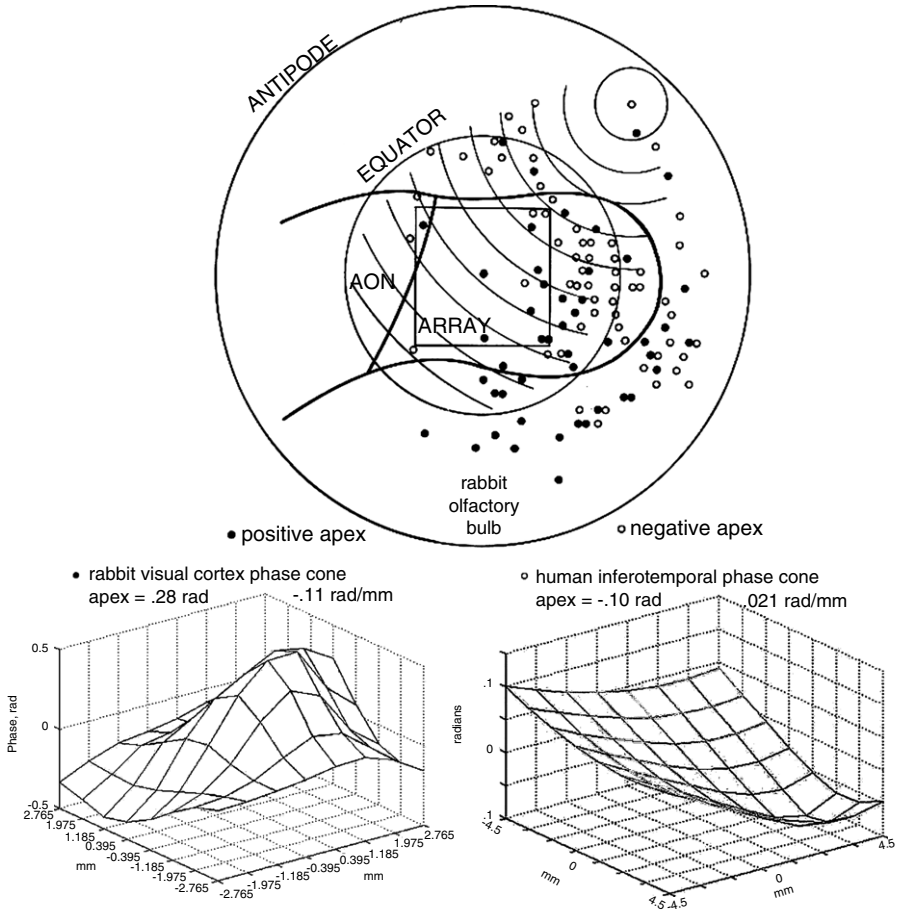

Fig. 4. The silhouette shows the outline of the olfactory bulb, on which is superimposed a 4 × 4 mm rectangle giving the position of the surgically placed 8 × 8 electrode array. The two circles specify the flattened surface of the spherical bulb. The solid and open dots show the locations of conic apices. The arcs show the isophase contours of one phase cone at 0.1 rad intervals (Breiman, 1968). The insets below the display of apices give examples of phase cone respectively from rabbit (Freeman, 2004b), phase lead, and human (Freeman et al., 2006), phase lag.

(randomness) at the center frequency were small (Fig. 8B). More easily found were deviations in the side bands of the central added sine wave (Fig. 8A), in which the modal intervals were shorter than predicted by the Rayleigh distribution (see Figs. 6, 7 in Freeman (2009b)).

An opportunity presented itself to estimate the width of the endogenous bandwidth of the carrier waves of the ECoG segments that were classified with respect to the conditioned stimuli presented on the trials from which the ECoG came, carrying classifiable spatial AM patterns of amplitude modulation (Freeman, 2005, 2006). The AM patterns were measured at the maxima of analytic power in segments identified as having relatively constant analytic frequency between null spikes. The minimum value of the spatial standard deviation of the analytic frequency, $SD_X(t)$, in each frame between down spikes was used to estimate the analytic frequency distribution in Hz in that frame. Each value was paired in a scattergram with the interval duration expressed as its reciprocal, the analytic frequency in Hz (Fig. 9). The scattergram was repeated for ECoG bandwidths of 4, 8 and 16 Hz, with calculation of the geometric mean of the null spike rate, respectively 2.1±0.7 Hz, 3.8 ± 1.4 Hz, and 7.4 ± 2.6 Hz. The recurrence rate of classifiable frames was determined to lie within the theta range (3–7 Hz) (Freeman, 2005). Therefore, the optimal estimate of bandwidth when expressed as the minimal value of $SD_X(t)$ was inferred to be in the vicinity 8 Hz, giving a modal spike repetition rate near 5 Hz, in the middle of the theta range.

The Rayleigh distribution was calculated for the same length of data using either brown or black noise in the same filter settings, giving a globular distribution of points at the upper limit of the range of the ECoG (Fig. 9, "X"). The Rice distribution was calculated in the same way but after adding a sine wave to the noise at the center frequency of the pass band with RMS amplitude half the SD of the noise at that frequency. The points were distributed in a globular cluster at the lower end of the elliptical ECoG distribution. This finding indicated that the ECoG data contained non-random activity in the form of a narrow-band oscillation constituting a signal, which by inference may correspond to the relatively fixed carrier wave of the classifiable AM patterns. The clustering of the ECoG points overlaps the theta range (3–7 Hz). That can explain the neural mechanism for the tendency of bursts of gamma activity (variously defined in the range of 25–100 Hz to include low and high gamma) to recur at rates in the theta range, which is known as the *theta–gamma linkage* (Canolty et al., 2006; Chrobak & Buzsáki, 1998; Fell et al., 2003; Lisman, 2005; Schack, Vath, Petsche, Geissler, & Möller, 2002), and which appears to hold for beta activity (12.5–30 Hz) as well (Freeman, 2005).

The fact that adding power at a fixed frequency to brown or black noise prolongs the intervals between null spikes in that pass band is significant, because the hallmark of frames between null spikes, which carry AM patterns that are classifiable with respect to conditioned stimuli, is that they have long durations, long enough to encompass 3 to 5 cycles of the carrier frequency for read-out (Fig. A1.08, C in Freeman (2004a)). These frames last much too long to be modeled with random numbers, i.e., random noise (Freeman, 2006).

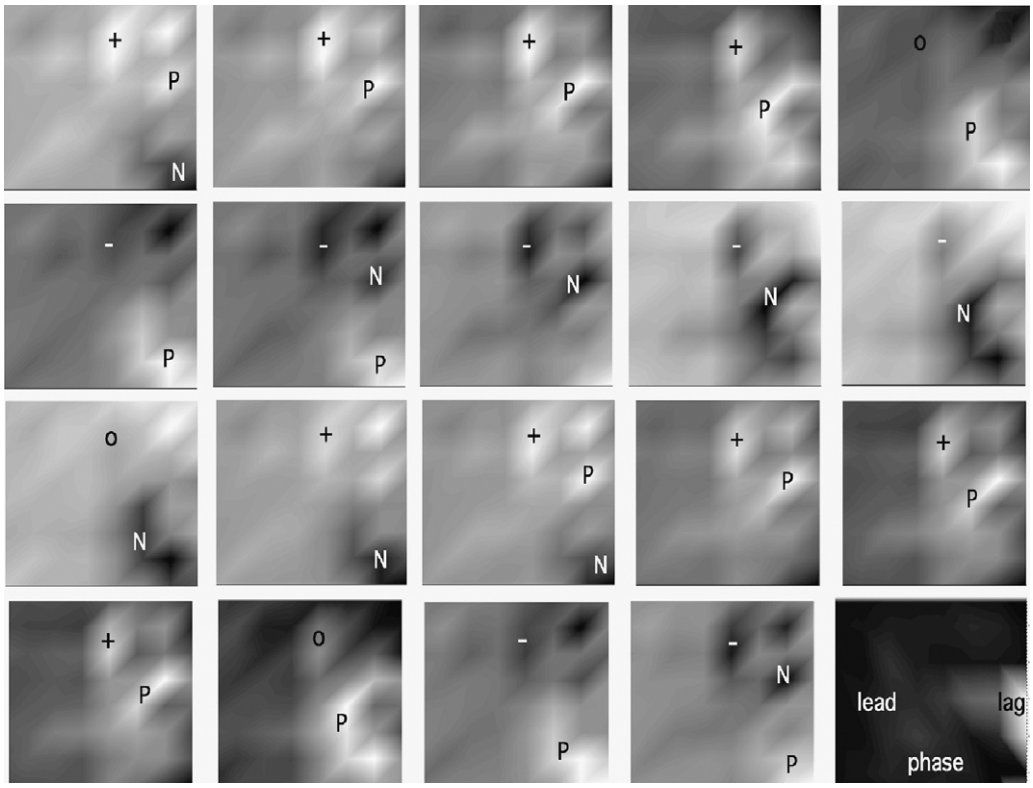

Fig. 5. Frames from a 5.6 × 5.6 mm 8 × 8 electrode array were shown in time steps of 4 ms (left to right, top to bottom) of ECoG filtered in a pass band 20–25 Hz. A small focus (+o − o+) oscillated in place with cycle duration near 48 ms, the other focus rotated counterclockwise with cycle duration near 46 ms. Each pattern persisted for several cycles, then terminated. Four to six independent phase-locked ECoG patterns commonly overlapped, giving the appearance of a pan of boiling water (Freeman, 2004b; Kozma & Freeman, 2008). From a lecture by WJF at DICE, Castiglioncello, Italy 28 Sept 2008.

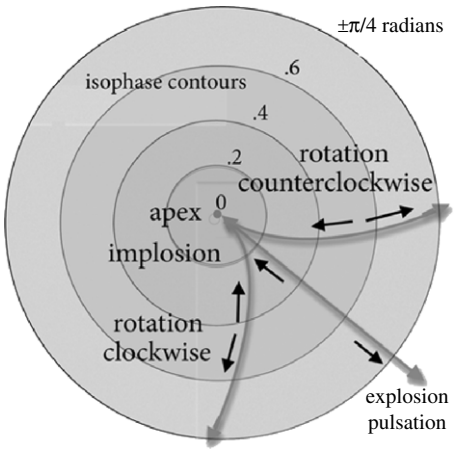

Fig. 6. Summary diagram of observed conic phase gradients with time variation appearing as vortices: either inward (implosion, maximal lag at the apex) or outward (explosion, maximal lead at the apex); rotation clockwise; rotation counterclockwise; or pulsation without rotation (Freeman & Vitiello, 2009; Kozma & Freeman, 2008). From a lecture by WJF, DICE Conf, Castiglioncello, Italy 28 Sept 2008.

4. Origin and stabilization of the background

The PSD slopes steeper than -2 cannot be simulated by summing white noise. Instead, it is necessary to sum the simulated impulse responses that are triggered by simulated pulses in a Poisson process governed by random numbers. The envelope of the evoked unit activity (Fig. 10) gives the kernel of integration for ECoG. The impulse response is adequately simulated with the sum of two exponential terms, one for the rise rate and the other for the decay rate, thus neglecting higher order poles. The rise rate determines the slope of the PSD, and the decay rate determines the break frequency, below which the spectrum tends to be flat (Freeman & Zhai, 2009). Excitatory input drives cortex above its self-regulated set point that determines the background level. The increased activity increases the decay rate and decreases the rise rate, owing to saturation of forward gain of neural populations by the refractory periods. The saturation or partial block diminishes the positive feedback gain (gain contours in Fig. 11). The same result holds for decreasing the set point, which decreases the background activity. The saturation effect depends on the ratio of evoked activity to the background activity. For example, the reduction in spike activity with the onset of slow wave sleep reflects the reduction in the set point with reduced arousal, and this can then explain the steeper slope of the PSD in slow wave sleep.

The power-law distribution of energy of frequencies requires that there be a comparable source of distribution in the delays in the neural negative feedback loops that determine the frequencies. The local feedback delays from propagation times are negligible, so the frequencies are determined by the rise rates of the dendritic cable delays but mainly by the decay rates of the passive membranes. These frequencies are in the gamma range (Freeman, 1975, 2006). Lower frequencies in the beta range involve longer delays contributed by longer propagation delays. The power-law distribution of frequencies is provided by the distributions of the lengths of intracortical axons that run parallel to the surface, which on re-evaluation have also been shown to be power-law and not exponential (Freeman, 2007a).

The key experimental evidence for this hypothesis has come from studies of the impulse response of a population of neurons at the input to the olfactory bulb, which on electrical stimulation of incoming axons shows a transient increase in the level of activity with no evidence for forward or recurrent inhibition (Fig. 10).

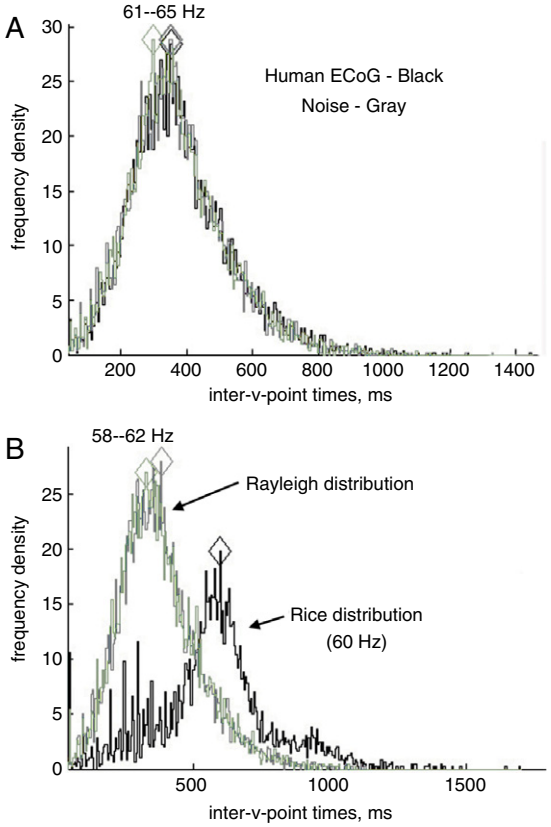

Fig. 7. A. Histograms of time intervals between down spikes are superimposed for ECoG (black) and for black and brown noises (gray). The ECoG were from a human subject in slow wave sleep (Fig. 1) digitized at 5 ms steps. The pass band of 4 Hz was stepped over the 19 s record. No deviations from the Rayleigh distribution were found except at spectral spikes located at 60 Hz and 80 Hz from line noise (spectral spikes in Fig. 1). B. The histogram centered at 60 Hz revealed as predicted the Rice distribution (Freeman, 2004b), which is from narrow band gamma oscillation that is superimposed on broad band background noise.

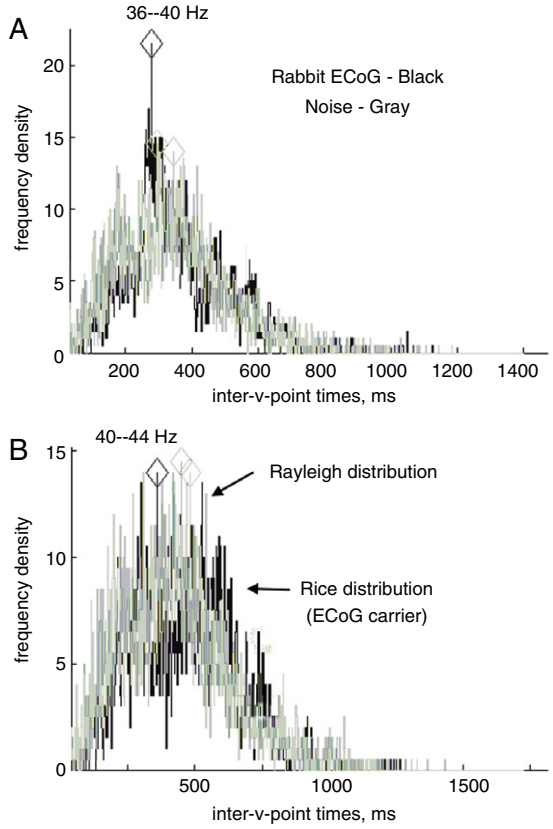

Fig. 8. A. The modal distributions of intervals calculated for rabbit ECoG, 2 ms digitizing step, and for simulated black noise and brown noise all conformed to Rayleigh distribution for bandwidths $\geq$8 Hz. B. The Rice distribution appeared in the ECoG from all 9 rabbits filtered in 4 Hz pass bands at center frequencies in the beta and gamma ranges, more commonly when subjects were responding to conditioned stimuli than when they were expectant or inactive (Freeman, 2009b).

Paradoxically the periglomerular neurons transmit to each other by GABA, which is widely shown to be an inhibitory transmitter in mammalian brains. However, these neurons have a high internal concentration of chloride ions (Siklós, Rickmann, Joó, Freeman, & Wolff, 1995), so the effect of GABA on GABA-A receptors is to open the channels and allow chloride to escape, thus depolarizing the membranes and causing excitation. An impulse input causes a transient increase in firing rate above the background level averaging about 10/s, followed by an exponential decay to the background without an overshoot. This is revealed by calculating post stimulus time histograms (PSTH) of trains of action potentials from representative neurons in the population on repetitive stimulation at low stimulus rates ($\leq$ 1/s) (Fig. 10).

When the impulse input intensity is increased, the response amplitude increases, and the rate of exponential decay likewise increases, as shown by 2 of 6 samples. The decay rates are determined by fitting the solutions to two coupled third order ordinary differential equations (ODE) (Fig. 11) that represent the dynamics of two subpopulations in the excited cortical population: a receiving subset and a transmitting subset that is continually renewed from the receiving subset (Freeman, 2009b).

The interaction strength is represented by the positive feedback gain, Kp, and the open loop dynamics is evaluated by three exponential terms: the passive membrane decay rate, the rise time imposed by the cable delay of the dendrites, and a concave upward deflection caused by the synaptic delay from axon to dendrite. The repeated solution of the equations with incremental increase in Kp gives a root locus plot (Fig. 11), in which the decay rates of

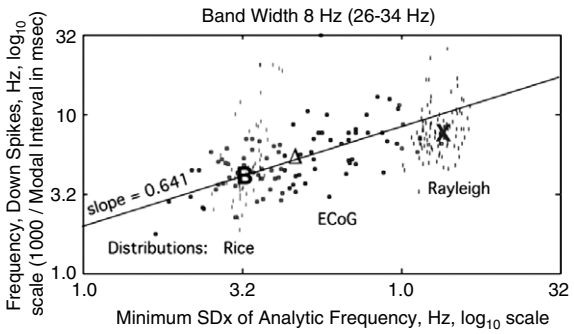

Fig. 9. The minimum of the spatial standard deviation of the analytic frequency from each of the 64 filtered ECoG signals was calculated in Hz. The instantaneous frequency of the down spikes was calculated by dividing 1000 by the interval between successive down spikes in ms and dividing that by 2π. The ECoG points in log–log coordinates fell in an elliptical distribution, which corresponded to the Rice relation about the geometric mean "Δ" between bandwidth and down spike frequency. The same analysis applied to black noise "B" and brown noise "X" yielded globular clusters at the two ends of the ECoG distribution (Freeman, 2009b).

the impulse responses give poles on the negative real axis of the complex plane. These locations along the root locus show that with increasing stimulus intensity, or with decreasing self-stabilized background activity, the feedback gain, Kp, is reduced.

The impulse response amplitude decreases in proportion with the stimulus intensity to zero response at threshold. The decay rate likewise decreases in proportion with the stimulus intensity and extrapolates to zero at threshold (Fig. 12).

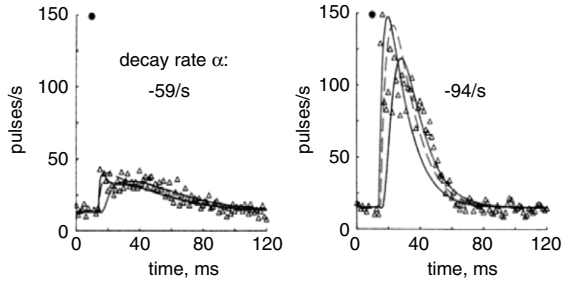

Fig. 10. The PSTH of a periglomerular neuron is shown for two representative intensities of stimulation. The data as plotting symbols were fitted with the solutions to a 6th order linear ODE with a variable coefficient, the positive feedback gain, Kp (Freeman, 1975).

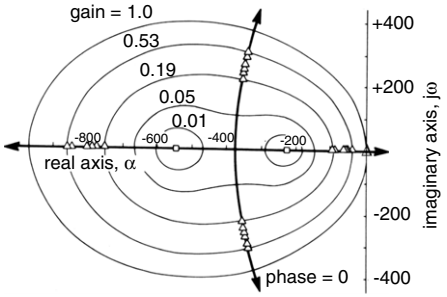

Fig. 11. Two 3rd order ODE are coupled with positive feedback gain, Kp, to model the dynamics of a population of excitatory neurons that sustain background activity. Six sets of the 4 of 6 poles closest to the imaginary axis are shown as Δ for 6 levels of intensity; two more sets for the highest frequencies are far to the left in the complex plane. The pole at the origin, Δ, is by extrapolation to amplitude = 0, decay rate = 0, Kp = 1.0 (from Fig. 5.13(a) on p. 292 in Freeman (1975)).

At zero decay rate the feedback gain is unity, Kp = 1. This finding implies that the background activity is governed by a point attractor, which is symbolized by the zero eigenvalue in the linear approximation to the nonlinear ODE, giving a pole Δ at the origin of the complex plane. The synaptic connection density is sufficiently high that, once it has begun by any random firing of a neuron, the activity is self-sustained indefinitely. Its set point and steady state level are regulated by neurohumoral control from aminergic nuclei in the brain stem (Freeman, 2005) that control the level of arousal. The model predicts the steady state at unity gain. Activity driven above the set point is homeostatically reduced. Decreases from loss of input are met by transient increases in gain Kp > 1, with return to the steady state. Proof is by showing that occluding the nostrils to block olfactory receptor input or cutting the olfactory nerve does not abolish the background activity (Freeman, 2009b).

5. Role of inhibition in generating oscillations

Further information about stabilization of background activity has been derived by simultaneously recording the ECoG at the cortical surface above a microelectrode and the train of action potentials generated by a single neuron embedded in populations of excitatory and inhibitory neurons (Freeman, 2009b; Freeman & Erwin, 2008). The ECoG is superior to local field potentials (LFP) from the depth electrode, because the phase relations between the two time series are more clearly defined. The question is asked, what is the relation between the pulse time series and the wave time series? Calculating the pulse probability conditional on ECoG amplitude provides the answer. Typically in the background state the amplitude histogram of the ECoG approximates the Gaussian normal density function, and the autocorrelation decays to zero with oscillations over distributions of frequencies. The spike trains likewise give autocorrelation functions that rise from zero to a sustained level showing the refractory periods, then steady state background activity. Interval histograms show an exponential decay to zero conforming to a Poisson process with a dead time at shortest intervals >0 that are caused by absolute refractory periods (Freeman, 1975).

The normalized conditional pulse probability density function has been fitted with an equation derived by a statistical generalization of the Hodgkin–Huxley equations (Freeman, 2009b; Freeman & Erwin, 2008). The derivative of the asymmetric sigmoid curve, dp/dv, gives the nonlinear gain (Kp, Fig. 13A). There are two values of the wave amplitude at which unity gain occurs. The KIe excitatory set stabilizes itself to the right of maximal gain. Further increases result in decreased gain, Kp, as shown by the tangents to the sigmoid curve (Fig. 13A) as evaluated in Fig. 10 and derived in Fig. 11.

Cortex is composed of mixed populations of excitatory and inhibitory neurons. They stabilize themselves at unity gain well below maximal gain (Fig. 13B), so that impulse driving tends transiently to increase the gain. However, cortex maintains itself at or near a state of criticality (Bressler & Kelso, 2001; Freeman, 2008; Freeman et al., 2001; Kozma & Freeman, 2008; Kozma et al., 2005) by the saturation modeled with the point attractor that is symbolized by the pole at the origin of the complex plane (Δ in Fig. 11). The negative feedback gives rise to oscillatory impulse responses (evoked potentials). They reveal the cortical operating point, for which the frequency and decay rate are amplitude-dependent, owing to bilateral saturation imposed by thresholds during excess inhibition and the refractory periods during excess excitation. Impulse responses that exceed in amplitude the peak-to-peak amplitude of the self-stabilized background activity (Mode 1e and 1i in Fig. 14) tend always to lower frequencies or faster decay rates or both, owing to the limitations imposed by the refractoriness of trigger zones on forming action potentials under the influence of the synaptic currents from dendrites.

Owing to the mixed populations there are three kinds of feedback in cortex: negative, Kn, positive excitatory, Ke, and positive inhibitory, Ki. All three gains are modified by changes in response amplitude, but in different ways. These are illustrated by root loci in the complex plane as a function of the three gains, starting at the three poles as in Fig. 11, representing the open loop rate constants that are essentially the same for excitatory and inhibitory neural populations (Freeman, 2009b). The root loci extend outwardly into the complex plane to zeroes typically far distant from the origin. In all cases the nonlinear sigmoid input–output relation in Fig. 13 governs the functions. The root loci are plotted only in the upper half of the complex plane near the origin; the lower half is a mirror image. The curve in Fig. 14 running upwardly to the right across the imaginary axis represents the locus of predicted frequencies and decay rates of impulse responses in conditions of cortical dynamic symmetry, when the two positive feedback gains are equal to Kn, which results in pole-zero cancellation and reduction in the network to one negative feedback loop, the reduced KII set (Freeman, 2009b; Freeman & Erwin, 2008).

Two Modes of deviation from symmetry by explicit symmetry breaking are illustrated in Fig. 14. In Mode 1e the input that excites the bulb through electrical stimulation of the olfactory nerve, the sensory afferent pathway from the receptors, activates both the periglomerular neurons and the negative feedback loop. The input of the excitatory interneurons to the loop sustains an excitatory bias. The effect (Mode 1e) is to rotate the root locus clockwise, so that increased amplitude gives increased decay rate with constant frequency. In Mode 1i the stimulation of the output axons likewise excites the negative feedback loop but also the inhibitory interneurons, which creates an inhibitory bias and frequency dispersion especially into the low frequency range, with

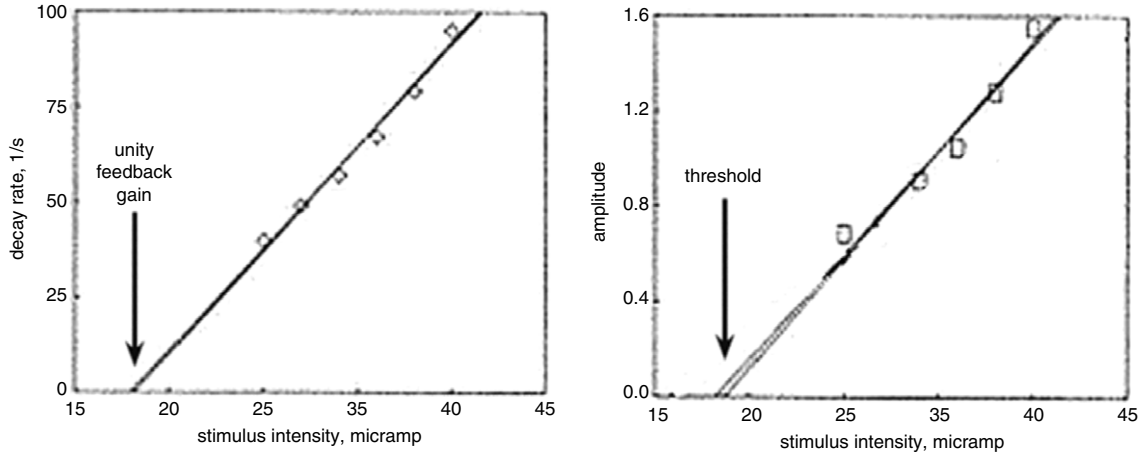

Fig. 12. Extrapolation to zero amplitude at threshold gives zero decay rate and unity gain in accord with root loci in Fig. 14 Freeman (1975).

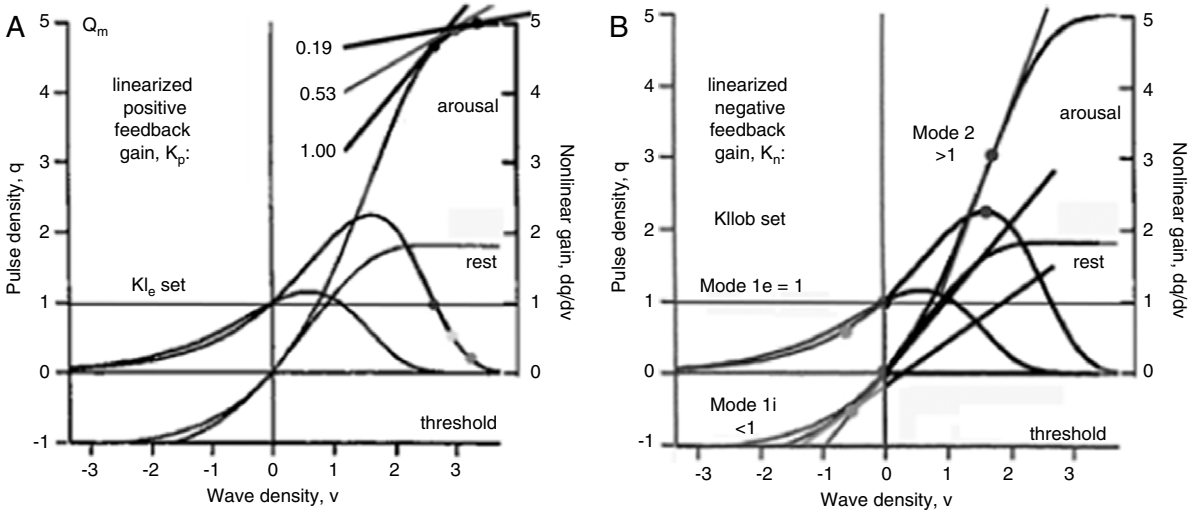

Fig. 13. The nonlinear function that governs the probability of pulse firing conditional on dendritic current intensity and ECoG wave amplitude holds for both excitatory and inhibitory populations. A. Mutual excitation (KIe set). B. Negative feedback (KII set (Freeman, 2005)). Two sigmoid curves and their gain curves are shown for two behavioral states: rest and arousal, governed by the maximum normalized pulse density $Q_m = 2$ at rest and 5 at work (Freeman & Erwin, 2008).

diminished cortical output through the spatiotemporal integration that is imposed by the output pathway. Increased input intensity decreases the frequency with little change in decay rate. Thus there are multiple determinants of the spectral content of the ECoG under differing conditions and sources of input.

The salient finding is the symmetry in the background state in the absence of impacts from sensation or intention, so that the frequencies are for the most part collapsed into a very simple spectrum. In this state the power spectral density of the ECoG and EEG tends to a power-law form, in which all frequencies are present but not as peaks above the straight line. The values of the slope in awake states typically cluster slightly steeper than -2 (slope $= -2$ is *brown* noise). In slow wave sleep the slope steepness to -3 or steeper (which is referred to as *black* noise (Freeman & Zhai, 2009)).

6. Evidence for control by a limit cycle attractor

While the dynamics of cortex in Mode 1 is dominated by the move toward stabilization under bombardment that drives cortex outside its self-stabilized range, within that range the activity reveals a very different dynamics in the spontaneous variation of the frequency and decay rate of the impulse response to fixed stimulus intensity. Modeling the root loci that conform to the variations has shown that the dynamics designated as Mode 2 is dominated by the move toward destabilization by the approach to the imaginary axis with increasing amplitude, the reverse of Mode 1. The root loci for various combinations of Kn, Ke and Ki cross the axis but then curve back and re-cross the axis at a point of convergence, which corresponds to a complex conjugate pole pair on the axis, implying the presence of a limit cycle attractor (Fig. 15).

Changing the background or the input changes the evoked potentials along the same root loci (Freeman, 2009b), which indicates that the underlying factor that brings the operating point toward the imaginary axis is not the increase in the response amplitude, which is an effect of the closer approach of the operating point to the limit cycle attractor. It is apparent that the factor that carries the dynamics toward the boundary of stability is the decrease in the amplitude of the background activity. Once the operating point has been shifted by noise reduction across the imaginary axis into the domain of positive real exponents, the move to the limit cycle attractor is inexorable, suggesting that the destabilization of the cortex by the combination of the conditioned stimulus and a null spike may drive the cortex to a singularity.

7. Conclusion

The remainder of this brief overview is devoted to asking and answering five questions. What is an optimal description of the expectant brain state? What factor might lower background

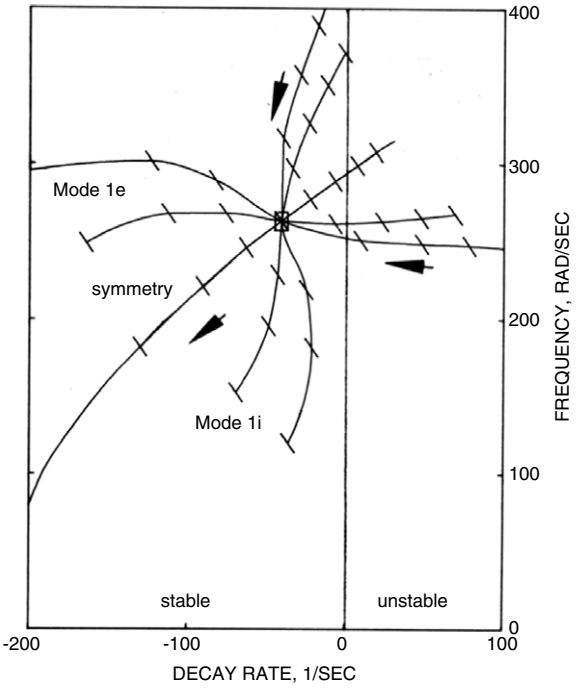

Fig. 14. This root locus diagram shows only the most critical root close to the origin of a complex conjugate pair with a mirror image below. The center of the star represents the background state that is maintained by the point attractor in Fig. 11. That state is symmetric by pole-zero cancellation of the two positive feedback loops. The deviations from symmetry occur on different types of inputs. In this Mode 1, increased amplitude usually yields increased stability, as indicated by the arrows showing the direction of change with increased amplitude or decreased background level (see Fig. 6.7 in Freeman (1975)).

amplitude that induces the move of the operating point toward instability? What mode of description can best express the change in state that is implied by an approach of the operating point toward a singularity in the piece-wise linear analysis of the dynamics? What factor might provide an activation energy that is required to cross the imaginary axis? How is an activated cortical pattern read-out and transmitted broadly through the forebrain?

The proposed answers to the five questions are as follows. First, the best description of the cortex in an expectant state is that cortex holds itself at its dynamic operating point in or near a state of criticality that is rightly described as self-organized, because it is homeostatically controlled (Freeman, 2008). Studies of this state provide important parameters of cortical dynamics such as the PSD, the axon connectivity, and the size and durations of areas of activity, having power-law distributions that support self-similarity across wide spatial and temporal scales. Observations of the textures of the spatiotemporal patterns of phase and amplitude of the ECoG show that they resemble the bubbles in a pan of boiling water (Freeman, 2004a, 2004b), so that they manifest the maintenance of a non-equilibrium steady state with prodigious expenditure of metabolic energy. Most importantly, cortex has pluripotentiality for very rapid changes among recurring patterns that extend over broad cortical areas (Pribram, 2009), which may reflect the continual retrieval and actualization of memories from the knowledge base of the brain.

Second, the neural mechanism that precipitates the reduction in background activity appears to be a down spike from interference in a pass band that is selected by input or by a local fluctuation, which breaks the symmetry of the critical state at the operating point (small rectangle centered in Fig. 14). The theta gating frequency that is seen in the recurrence of spatial AM patterns in relation to the relative frequencies in analytic power histogram in Fig. 3B suggests that the threshold for an effective null spike may be $< 10^{-4}$ of maximal mean power. The spatiotemporal distributions of the null spikes in Fig. 2C suggest that the spatial location might be anywhere within the sensory cortex, which is consistent with the variation in spatial location of the apices of phase cones accompanying the AM patterns (Freeman, 2004a; Freeman et al., 2006).

Third, the event that constitutes the emergence of each new AM pattern with its accompanying stable analytic phase pattern is best described as a phase transition, which in a dissipative system such as cortex is the selection by the stimulus of one among a collection of unitarily inequivalent ground states (Freeman & Vitiello, 2006; Vitiello, 2001). These states are held *in potentia* by synaptic networks that have been modified in prior learning, and that are brought close to threshold for activation by preafferent signals under limbic control in the process of selective attention. When activated, they constitute a landscape of chaotic attractors, each corresponding to one of several possible or plausible expected answers to a question that an animal or human asks with each act of observation.

Fourth, the sensory cortices maintain a high degree of selectivity in responding only to desired or expected stimuli based in experience, so it is plausible to suppose that the many null spikes that recur asynchronously in a Rayleigh spectral continuum merely open a gate for a possible phase transition. A suggested mechanism is that prior learning over repeated presentations of a conditioned stimulus forms a Hebbian nerve cell assembly that serves as a correlation map for the pairwise activated neurons. Any subset that is excited then activates the entire microscopic assembly, constituting an inductive generalization from the individual to the class. The firing of such neuron assemblies can be sustained for many tens of ms, as has repeatedly been demonstrated in unit spikes in all sensory cortices by many neurobiologists using microelectrode recording of feature detector neurons. The null spike may initiate the phase transition that transposes the activity across levels, from the microscopic activity of the assembly to the mesoscopic activity of the entire sensory cortex into a wave packet, which is a mechanism that can integrate past learning with the present state into a percept.

Fifth, the input to sensory cortex is carried on pathways by topographic mapping, whereas cortical output is transmitted not only by mapping but by divergent–convergent projections that perform a spatiotemporal integral transformation, which is comparable to that in holography (Pribram, 2009) though without an inverse transform. The anatomical tracts resemble the wiring diagram in an analog crosscorrelator. This operation selects the spectral component of the transmitted signal that has the same instantaneous frequency, which is the carrier of the endogenously constructed mesoscopic AM pattern, while it deletes the signals with dispersed frequency and phase, which are the microscopic raw sense data. As in a hologram, every fraction of the cortical output carries the same signal, so this operation interfaces the cortical input and the cortical output, each with its own developmental and anatomical constraints. Every fraction of the output undergoes the same enhancement of signal-to-noise ratio in each transmission. These several attributes attest to the utility of the transposition from microscopic pulse frequencies (sensations) to mesoscopic pulse and wave densities (perceptions).

These operations are feature binding on a grand scale. The interpretation from theoretical physics is that the populations in cortex, by widespread, continuously distributed synaptic interaction, generate an order parameter, which is a collective force that epiphenomenally manifests itself in the ECoG, as it imposes mesoscopic patterned order on the microscopic neurons sustaining it. During a null spike, the order parameter transiently diminishes close to zero. When the populations are momentarily freed from order into disorder, an active Hebbian assembly may capture the whole and direct the cortical trajectory across

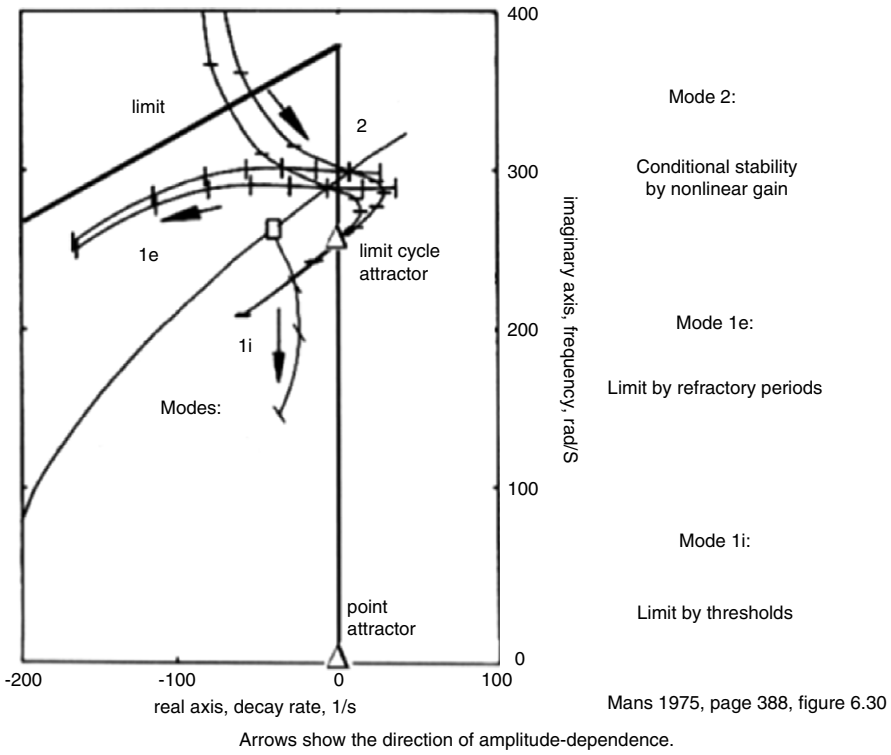

Fig. 15. Examples are shown of the root loci in Mode 2, in which the cortical impulse responses remain inside the bounds that are prescribed by the nonlinear function in Fig. 13B, and by the operation of the point attractor derived in Fig. 11. The convergence of the root loci to crossing the imaginary axis at or near a point with increasing response amplitude and decreasing background activity indicate the presence of a limit cycle attractor in the near vicinity of the self-stabilized operating point symbolized by the small rectangle (Fig. 6.21, p. 374 (Freeman, 1975)).

the attractor landscape to the relevant basin of attraction, initiating narrow band oscillation. Thereafter the neurons are mobilized and constrained into the construction of a new AM pattern that actualizes and broadcasts the knowledge that the cortex holds about the selecting stimulus at the carrier frequency. The endogenous trigger of the transition, which emerges from the random activity, the null spike, justifies the description of the phase transition as spontaneous breaking of symmetry (Freeman, 2008; Freeman & Vitiello, 2006). The memory store is an indefinitely large collection of latent ground states. The maintenance and the mobilization of the knowledge store depend intrinsically and unavoidably on energy dissipation (Freeman, 2008; Freeman & Vitiello, 2006) by the brain, as measured by fMRI and related techniques to estimate cerebral blood flow.

These are the new experimental data and some heuristic hypotheses to explain them (Freeman, 1975; Freeman, Kozma, Bollobás, & Ballister, 2009; Freeman & Vitiello, 2009; Pribram, 2009). What is needed now is development of rigorous mathematics on which to base a proper theory of perception.

Acknowledgments

Recognition is owed to Brian Burke, Jose Rodríguez, and William Redfearn for meticulous programming in Matlab.

References

Breiman, L. (1968). *Probability*. Reading, MA: Addison-Wesley.
Bressler, S. L., & Kelso, J. A. S. (2001). Cortical coordination dynamics and cognition. *Trends in Cognition Science*, (5), 26–36.
Canolty, R. T., Edwards, E., Dalal, S. S., Soltani, M., Nagarajan, S. S., & Kirsch, H. E. (2006). High gamma power is phase-locked to theta oscillations in human neocortex. *Science*, *313*(5793), 1626–1628.
Chrobak, J. J., & Buzsáki, G. (1998). *Gamma oscillations in the entorhinal cortex of the freely behaving rat Journal of Neuroscience*, *18*(1), 388–393.
Fell, J., Klaver, P., Elfadil, H. E., Schaller, C., Elger, C. E., & Fernández, G. (2003). Rhinal–hippocampal theta coherence during declarative memory formation: interaction with gamma synchronization?. *European Journal of Neuroscience*, *17*(5), 1082–1088.
Freeman, W. J. (1975). *Mass action in the nervous system*. New York: Academic Press, ©WJF 2004. http://sulcus.berkeley.edu/MANSWWW/MANSWWW.html.
Freeman, W. J. (1990). On the problem of anomalous dispersion in chaoto-chaotic phase transitions of neural masses, and its significance for the management of perceptual information in brains. In H. Haken, & M. Stadler (Eds.), *Synergetics of Cognition*: *vol. 45* (pp. 126–143). Berlin: Springer-Verlag, Chapter.
Freeman, W. J. (2000). A proposed name for aperiodic brain activity: Stochastic chaos. *Neural Networks*, *13*, 11–13. http://sulcus.berkeley.edu/wjf/BD.Stochastic.chaos.name.pdf.
Freeman, W. J. (2004a). Origin, structure, and role of background EEG activity. Part 1. Analytic amplitude. *Clinical Neurophysiology*, *115*, 2077–2088. http://repositories.cdlib.org/postprints/1006.
Freeman, W. J. (2004b). Origin, structure, and role of background EEG activity. Part 2. Analytic phase. *Clinical Neurophysiology*, *115*, 2089–2107. http://repositories.cdlib.org/postprints/987.
Freeman, W. J. (2005). Origin, structure, and role of background EEG activity. Part 3. Neural frame classification. *Clinical Neurophysiology*, *116*(5), 1118–1129. http://repositories.cdlib.org/postprints/2134/.
Freeman, W. J. (2006). Origin, structure, and role of background EEG activity. Part 4. Neural frame simulation. *Clinical Neurophysiology*, *117*, 572–589. http://repositories.cdlib.org/postprints/1480/.
Freeman, W. J. (2007a). Scale-free neocortical dynamics. *Scholarpedia*. http://www.scholarpedia.org/article/Scalefree_neocortical_dynamics.
Freeman, W. J. (2007b). Hilbert transform for brain waves. *Scholarpedia*, http://www.scholarpedia.org/article/Hilbert_transform_forbrain_waves.
Freeman, W. J. (2008). A pseudo-equilibrium thermodynamic model of information processing in nonlinear brain dynamics. *Neural Networks*, *21*, 257–265. http://repositories.cdlib.org/postprints/2781.
Freeman, W. J. (2009a). Cortical mechanisms of memory formation and readout. *Proc. IJCNN*, Abstract #107.
Freeman, W. J. (2009b). Deep analysis of perception through dynamic structures that emerge in cortex from self-regulated random noise. *Cognitive Neurodynamics*, *3*(1), 105–116. http://www.springerlink.com/content/v375t5l4t065m48q/.
Freeman, W. J. (2005). NDN, volume transmission, and self-organization in brain dynamics. *Journal of Integrative Neuroscience, 4*, *4*, 407–421.
Freeman, W.J. (2008). Freeman's Mass Action, *Scholarpedia*. http://www.scholarpedia.org/article/Freeman%27s_mass_action.
Freeman, W. J., & Baird, B. (1987). Relation of olfactory EEG to behavior: Spatial analysis. *Behavioral Neuroscience*, *101*, 393–408.
Freeman, W. J., & Erwin, H. (2008). Freeman K-set. *Scholarpedia*. http://www.scholarpedia.org/article/Freeman_K-set.

Freeman, W. J., Holmes, M. D., West, G. A., & Vanhatalo, S. (2006). Fine spatiotemporal structure of phase in human intracranial EEG. *Clinical Neurophysiology*, *117*(6), 1228–1243.

Freeman, W. J., Kozma, R., Bollobás, B., & Ballister, P. (2009). Scale-free cortical planar networks. In B. Bollobás, R. Kozma, & D. Miklös (Eds.), *Handbook Large-Scale Random Networks*: *vol. 18*. NY: Springer. http://www.springer.com/math/numbers/book/978-3-540-69394-9.

Freeman, W. J., Kozma, R., & Werbos, P. (2001). Biocomplexity: Adaptive behavior in complex stochastic dynamical systems. *BioSystems*, *59*, 109–123.

Freeman, W. J., O'Nuillain, S., & Rodriguez, J. (2008). Simulating cortical background activity at rest with filtered noise. *Journal of Integrative Neuroscience*, *7*(3), 337–344.

Freeman, W. J., & Vitiello, G. (2006). Nonlinear brain dynamics as macroscopic manifestation of underlying many-body field dynamics. *Physics of Life Reviews*, *3*, 93–118. doi:10.1016/j.plrev.2006.02.001.

Freeman, W. J., & Vitiello, G. (2009). Dissipative neurodynamics in perception forms cortical patterns that are stabilized by vortices. *Journal of Physics Conf Series*, *174*, 012011. http://www.iop.org/EJ/toc/1742-6596/174/1.

Freeman, W. J., & Zhai, J. (2009). Simulated power spectral density (PSD) of background electrocorticogram (ECoG). *Cognitive Neurodynamics*, *3*(1), 97–103. doi:10.1007/s11571-008-9064-y.

Kozma, R., & Freeman, W. J. (2001). Chaotic resonance: Methods and applications for robust classification of noisy and variable patterns. *International Journal of Bifurcation and Chaos*, *10*, 2307–2322.

Kozma, R., & Freeman, W. J. (2008). Intermittent spatio-temporal desynchronization and sequenced synchrony in ECoG signals. *Chaos*, *18*, 037131. doi:10.1063/1.2979694. Special Issue: Synchronization in Complex Networks, J. Suykens, G. Osipov (Eds.).

Kozma, R., Puljic, M., Balister, P., Bollabás, B., & Freeman, W. J. (2005). Phase transitions in the neuropercolation model of neural populations with mixed local and non-local interactions. *Biological Cybernetics*, *92*, 367–379. http://repositories.cdlib.org/postprints/999.

Lisman, J. (2005). The theta/gamma discrete phase code occurring during the hippocampal phase precession may be a more general brain coding scheme. *Hippocampus*, *15*(7), 913–922.

Makeig, S., Westerfield, M., Jung, T.-P., Enghoff, S., Townsend, J., & Courchesne, E. (2002). Dynamic brain sources of visual evoked responses. *Science*, *295*, 690–694.

Papoulis, A., & Pillai, S. U. (2002). *Probability, random variables, and stochastic processes* (4th Ed.). Boston: McGraw-Hill.

Pribram, K. H. (2009). Holonomic brain theory. *Scholarpedia*, *2*(5), 2735. http://www.scholarpedia.org/article/holonomic_brain_theory.

Rapp, P. (1993). Chaos in the neurosciences: Cautionary tales from the frontier. *Biologist*, *40*, 89–94.

Rice, S. O. (1945). Mathematical analysis of random noise. *Bell System Technical Journal*, *24*, 46–156. Section 3.10, pp. 98-10; (1948). *Bell System Technical Journal*, *27*, 109–157.

Schack, B., Vath, N., Petsche, H., Geissler, H.-G., & Möller, E. (2002). Phase-coupling of theta–gamma EEG rhythms during short-term memory processing. *International Journal of Psychophysiology*, *44*(2), 143–163.

Siklós, L., Rickmann, M., Joó, F., Freeman, W. J., & Wolff, J. R. (1995). Chloride is preferentially accumulated in a subpopulation of dendrites and periglomerular cells of the main olfactory bulb in adult rats. *Neuroscience*, *64*, 165–172.

Vitiello, G. (2001). *My double unveiled*. Amsterdam: John Benjamins.